Natural killer cell behavior in lymph nodes revealed by static and real-time imaging

Marc Bajénoff,[1] Béatrice Breart,[2] Alex Y.C. Huang,[3] Hai Qi,[3] Julie Cazareth,[1] Veronique M. Braud,[2] Ronald N. Germain,[3] and Nicolas Glaichenhaus[1]

[1]Institut National de la Santé et de la Recherche Médicale, Université de Nice-Sophia Antipolis, E03-44, 06560 Valbonne, France
[2]Centre National de la Recherche Scientifique, Université de Nice-Sophia Antipolis, UMR6097, 06560 Valbonne, France
[3]Lymphocyte Biology Section, Laboratory of Immunology, National Institute of Allergy and Infectious Diseases, National Institutes of Health, Bethesda, MD 20892

Natural killer (NK) cells promote dendritic cell (DC) maturation and influence T cell differentiation in vitro. To better understand the nature of the putative interactions among these cells in vivo during the early phases of an adaptive immune response, we have used immunohistochemical analysis and dynamic intravital imaging to study NK cell localization and behavior in lymph nodes (LNs) in the steady state and shortly after infection with *Leishmania major*. In the LNs of naive mice, NK cells reside in the medulla and the paracortex, where they closely associate with DCs. In contrast to T cells, intravital microscopy revealed that NK cells in the superficial regions of LNs were slowly motile and maintained their interactions with DCs over extended times in the presence or absence of immune-activating signals. *L. major* induced NK cells to secrete interferon-γ and to be recruited to the paracortex, where concomitant CD4 T cell activation occurred. Therefore, NK cells form a reactive but low mobile network in a strategic area of the LN where they can receive inflammatory signals, interact with DCs, and regulate colocalized T cell responses.

CORRESPONDENCE
Marc Bajénoff:
bajenoff@ipmc.cnrs.fr

Abbreviations used: 2-P, two photon; EGFP, enhanced GFP; HEV, high endothelial venule; LN, lymph node; PNAd, peripheral node addressin.

NK cells play important roles in immunological processes, including early defense against pathogens and elimination of tumor cells (1, 2). In addition to these effector activities, several recent studies have provided functional evidence of cognate interaction between NK cells and DCs that might contribute to the regulation of adaptive immunity (3–6). For example, $CD8\alpha^+$ DCs were found to be essential for the expansion of $Ly49H^+$ NK cells during acute murine CMV infection (7). In vitro coculture of NK cells with DCs in the presence of microbial stimuli results in NK cell activation that is dependent on soluble factors as well as cell-to-cell contacts (4–6). Reciprocally, activated NK cells promote DC maturation in vitro, and the presence of NK cells contributes to the maintenance of $CD8\alpha^+$ DCs in the spleen during murine CMV infection (7).

Beyond these indirect indications that NK cells affect DCs and, hence, might influence T cell responses dependent on these cells, there is more direct evidence for a contribution of NK cells to coelicited T cell responses. NK cells are present, albeit at a very low frequency (0.2–0.4%), in the lymph nodes (LNs) of unimmunized animals, and studies have shown that activated NK cells can enter LN draining sites of immunization or infection, where they influence adaptive immune cell differentiation (8, 9, 10). Collectively, this body of work suggests that NK–DC–T cell interactions are likely to take place within the LN environment, affecting the fate of antigen-specific lymphocytes activated in the same tissue site. However, microscopic evidence of direct contact between NK cells and DCs in vivo has not been reported, and, thus, the location and characteristics of such contact, if it does occur, remain unknown.

LNs are compartmentalized and highly organized structures that form an interface between the blood and lymphatic systems (11, 12). Lymph is continuously drained to the LN via lymphatic vessels and percolates into

M. Bajénoff and B. Breart contributed equally to this work.
The online version of this article contains supplemental material.

the node via the subcapsular cortical sinuses and conduits before exiting via the medullary sinus (13). This allows lymph-borne molecules to be transported and transcytosed to high endothelial venules (HEVs), which are the entry site of blood lymphocytes (14). DCs form an extensive network that populates specific localizations in the LN (15). Intravital imaging has shown that T cells are extremely motile in the paracortex, making only transient contacts with DCs in the absence of specific foreign antigen (16, 17). B cells move more slowly than T cells but are motile rather than sessile in the absence of cognate antigen (16). DCs also show substantial movement as they enter the LN parenchyma from the subcapsular sinus, but a recent study indicates that these migrating DCs eventually join the existing DC network and limit their further migration (15). Whether lymphoid lineage NK cells resemble B and T cells with a persistent roving behavior or are less migratory and more akin to the DCs that have integrated into a network is unknown. It seems clear that the positioning and migratory behavior of different cells within lymphoid tissues is linked to their respective functions, so determining these parameters for NK cells in the resting state and after an infectious challenge should add substantially to our understanding of how these cells contribute to immune responses.

Leishmania major is a protozoan parasite that invades myeloid cells such as macrophages and granulocytes and causes cutaneous lesions in susceptible mice (18). Although *L. major* has been shown to induce T cell activation, it also induces NK cells to rapidly secrete IFN-γ, which, in turn, can influence the differentiated state of both DCs and T cells in the nearby environment and, hence, the characteristics of a developing adaptive immune response. Therefore, we have used *L. major* as a tool to compare the behavior of activated NK cells to naive/resting NK cells within organized lymphoid tissue in which primary T cell responses develop. In this study, we report the results of immunohistochemical and dynamic intravital imaging studies of NK cell localization and movement within the LNs of both naive and *L. major*–infected animals. Our findings indicate that NK cells form a largely fixed network localized in strategic areas of the LN where they interact with DCs. Upon activation, additional NK cells are recruited to the same region of the paracortex as the fixed network. The NK cells in this location produce cytokines that could influence adaptive immune responses involving the associated DCs and DC-bound T cells in the same local lymphoid environment.

RESULTS

In situ visualization of NK cells in LNs

As a first step in analyzing the intranodal distribution of NK cells, it was necessary to develop a staining protocol for the unambiguous identification of these cells in lymphoid tissues. Two mAbs stain murine NK cells on tissue sections: 4D11, which recognizes Ly-49G2 (19), and PK136, which reacts with NK1.1 (20). However, 4D11 stains only a subset of NK cells, and NK1.1 is only expressed in some mouse strains. CD49b is expressed at high levels by most NK cells in most mouse strains and only at low levels by a small subset of $CD3^+$ T cells (Fig. S1, A and B; available at http://www.jem.org/cgi/content/full/jem.20051474/DC1; reference 21). Therefore, we tested the anti-CD49b mAbs HMα2 and DX5 for their ability to stain NK cells in LN tissue sections and found that only HMα2 gave positive staining. To confirm the specificity of this staining, LN and spleen cells were sorted into highly purified $CD3^+$ $CD49b^+$ T cells and $CD3^-$ $CD49b^+$ NK subsets. T cells and NK cells were labeled with CMTMR and CFSE, respectively, and 5×10^6 cells of each were coinjected into recipient mice. LNs from these mice were sectioned and stained with HMα2 mAb. Although HMα2 mAb did not stain CMTMR-labeled T cells ($n = 30$), it did stain all CFSE-labeled NK cells ($n = 40$) as well as some $CFSE^-$ $CMTMR^-$ endogenous LN cells (Fig. S1 A). $CFSE^-$ $CMTMR^-$ $CD49b^+$ cells were either small, round cells exhibiting HMα2 surface staining or larger structures exhibiting typical HEV shapes (Fig. S1 A). Most of these large $CD49b^+$ structures were confirmed to be HEV by their positive staining with both HMα2 mAb and the HEV-specific mAb MECA-79 that binds to peripheral node addressins (PNAds; Fig. S1 C; reference 22). Staining LN sections from unmanipulated mice with both anti-CD3 and anti-CD49b mAb revealed that all $CD49b^+$ cells were $CD3^-$, suggesting that the $CFSE^-$ $CMTMR^-$ $CD49b^+$ small, round cells were endogenous NK cells (unpublished data). Finally, NK cell depletion using anti-asialo GM1 mAb abrogated single cell staining by CD49b while preserving staining of PNAd-positive structures, confirming the specificity of this mAb for NK cells (Fig. S1 D). Therefore, costaining with HMα2 and MECA-79 mAb could be used to identify $CD49b^+$ $PNAd^-$ NK cells in LN tissue sections.

NK cells reside in the paracortex and the medulla of LNs after entry via HEVs and make contacts with DCs

Having established a method for the identification of NK cells within LN tissue sections, we next sought to determine their precise anatomic localization. In naive mice, NK cells populate two different areas of the LN. As previously described, NK cells ($PNAd^-$ $CD49b^+$) were observed in the T cell area beneath and between B cell ($B220^+$) follicles (Fig. 1 A, top). Staining was also observed between the two T cell areas of the auricular LN (Fig. 1 A), a region that was positive for the lymphatic marker Lyve-1, thus defining the LN medulla (Fig. 1 B, top). Although single NK cells were identified in both the T cell area and the medulla, their exact distribution in these two areas was difficult to analyze in stained sections imaged at low magnification. To better address this issue, $CD3^-$ $CD49b^+$ NK cells were isolated from spleens and LNs because NK cells from these organs can home to recipient LNs after adoptive transfer (Fig. S2, A and B; available at http://www.jem.org/cgi/content/full/jem.20051474/DC1). After CFSE labeling, we adoptively transferred 10^7 of these purified NK cells into naive mice. The bright staining of CFSE-labeled NK cells allowed the precise localization of individual cells in these images. Host LNs were harvested

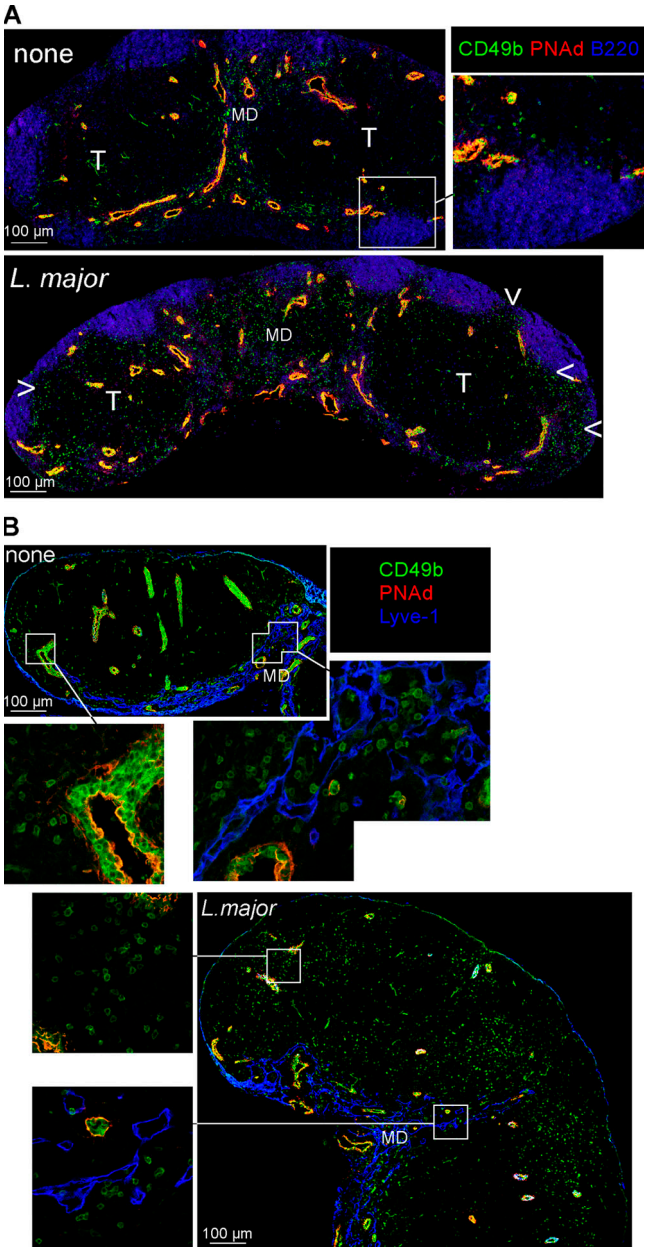

Figure 1. Distribution of NK cells in mice LNs. Mice were injected with *L. major* into the left ear and with PBS into the right ear. Left and right ear-draining LNs were collected 12 h after infection. Tissue sections from 10 individual LNs were analyzed for each condition by confocal microscopy. LN sections were stained for CD49b (green), PNAd (red), and either B220 (blue, A) or Lyve-1 (blue, B) to reveal the location of NK cells in relationship to the B cell follicles, HEVs, and the medulla (MD). Representative LN sections show the localization of NK cells in the paracortex and medulla of LNs draining either the infected (bottom) or contralateral ear (top). A representative picture for each group is shown. T, T cell zone. Arrows indicate regions of the LN where NK cells accumulate.

24 h after transfer, sectioned, and stained for B cell ($B220^+$) and lymphatic vessel ($Lyve\text{-}1^+$) markers (Fig. 2 a, left). As observed using CD49b staining, NK cells were present in both the T cell area and the medulla. Quantitative analysis of NK cell distribution indicated that 44% (211/483 cells counted) were present in the T cell area, and 56% were located in the medulla (Fig. 2 b, top). However, calculating the density of NK cells per millimeter squared revealed that NK cell density was higher in the medulla (62.3 cells/mm^2) than in the T cell area (22.8 cells/mm^2; Fig. 2 B, bottom). This explains why NK cells showed a more sparse distribution in the T cell area than in the medulla in tissue sections.

NK cells express L-selectin, which participates in T and B lymphocyte entry into LNs via HEVs. To examine whether L-selectin–expressing NK cells enter LNs in this manner, we injected CFSE-labeled NK cells i.v. into recipient mice. LNs were harvested 20 min later, and sections from these nodes were analyzed by confocal microscopy after staining with anti-PNAd mAb (Fig. S3 A, available at http://www.jem.org/cgi/content/full/jem.20051474/DC1). All observed CFSE-labeled cells were found to be associated with HEV at this time point. CFSE-labeled NK cells were then incubated for 30 min with either L-selectin–blocking or isotype control mAb before transfer i.v. into separate animals that were coinjected with additional L-selectin–blocking or isotype control mAbs. Spleens and LNs were harvested 5 h later to assess the number of $CFSE^+$ NK cells that entered these organs. NK cell homing to LN was reduced by 82%, suggesting that similar to blood-borne T and B cells, the entry of blood NK cells into LNs was mediated through HEVs in an L-selectin–dependent manner (23).

NK cells have been reported to interact with DCs in vitro (4, 5), and both NK cells and DCs were observed in the T cell area of human LNs (9). To look for evidence of direct NK–DC interactions in this and elsewhere in noninflamed LNs, tissue sections were stained with anti-CD49b, anti-CD11c, and anti-PNAd mAb. We found that $CD49b^+$ $PNAd^-$ NK cells and $CD11c^+$ DCs colocalized in the paracortex and the medulla (Fig. 3 A). To determine whether NK cells made contacts with these neighboring DCs, $CD49b^+$ $CD3^-$ NK cells were purified by flow cytometry, labeled with CFSE, and injected into naive mice. Out of 83 individually scored CFSE-labeled NK cells, 38 (46%) showed contact with large $CD11c^+$ cells in tissue sections (Fig. 3 B and Video 1, available at http://www.jem.org/cgi/content/full/jem.20051474/DC1).

Intravital imaging reveals DC contact and low motility of NK cells in noninflamed LNs

Because of the high density of DCs in the outer paracortex, it was not possible to determine by this static imaging method whether the observed NK cell–DC associations reflected specific interactions or merely random proximity as a result of cell packing. To address this issue, we used intravital two-photon (2-P) microscopy to assess the dynamics of possible NK–DC interactions in the superficial LN paracortex (<200 μm), as the medulla is inaccessible using this technology. I-Aβ–enhanced GFP (EGFP) knock-in mice were used as recipients to visualize endogenous LN DCs, which can be identified as $EGFP^{high}$ cells with dendritic morphology (24). Adoptive transfer of NK cells into these animals

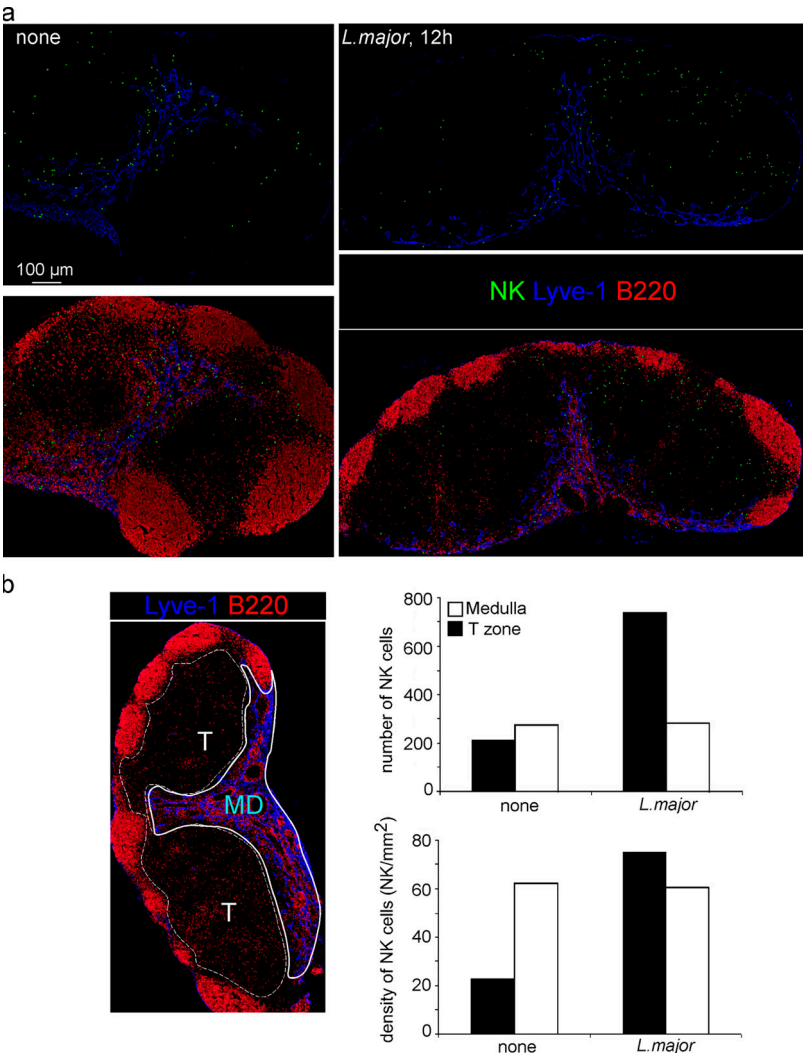

Figure 2. Quantification of NK cell distribution in LNs. BALB/c mice were injected with 10^7 CFSE-labeled NK cells. Recipient mice were injected or not injected with *L. major* in the ears. Ear-draining LNs were collected 12 h after infection. Tissue sections from eight individual LNs were analyzed for each condition by confocal microscopy. (a) LN sections were stained for B220 (red) and Lyve-1 (blue) to reveal the location of NK cells (green) in relationship to the B cell follicles and medulla. Representative LN sections show the localization of NK cells in the paracortex and the medulla of LNs draining either a control (left) or infected (right) site. (b) The total number (top graph) and density (bottom graph) of dye-labeled NK cells in the T cell zone (dashed line) and the medulla (MD; white line) were determined. T, T cell zone.

indicated that the NK cells interact with a diffuse network of MHC class II–positive cells (Fig. S4 and Video 2, available at http://www.jem.org/cgi/content/full/jem.20051474/DC1). However, similar to what has been recently described (15), the DC network visualized in I-Aβ-EGFP mice was very dense under the B cell follicles, precluding the observation of individual endogenous DCs. To overcome this problem, fluorescently labeled splenic DCs were injected subcutaneously into recipient mice that were also injected i.v. with labeled NK cells. This method allows the identification of single DCs and more precise assessment of the interactions these cells make with NK cells. Interactions between adoptively transferred NK cells and DCs were monitored intravitally 12 h later in the draining LN. Although the vast majority of dye-labeled NK cells were not in contact with transferred DCs presumably because they were interacting with the dense network of MHC class II^+ cells, a few NK cell–DC pairs were readily observed at the beginning of the imaging sessions. Out of 20 NK cells that were found in contact with dye-labeled DCs, 19 were found to unambiguously remain in contact with the DCs for at least 25 min (Fig. 3, C and D; and Video 3). Although ex vivo manipulated and adoptively transferred DCs cannot be equated with endogenous resting DCs, these real-time observations together with the static imaging data demonstrate that NK cells reside in specific areas of the LN where they interact with DCs. It is important to note that these data do not allow us to draw conclusions about the dynamic behavior of NK cells in

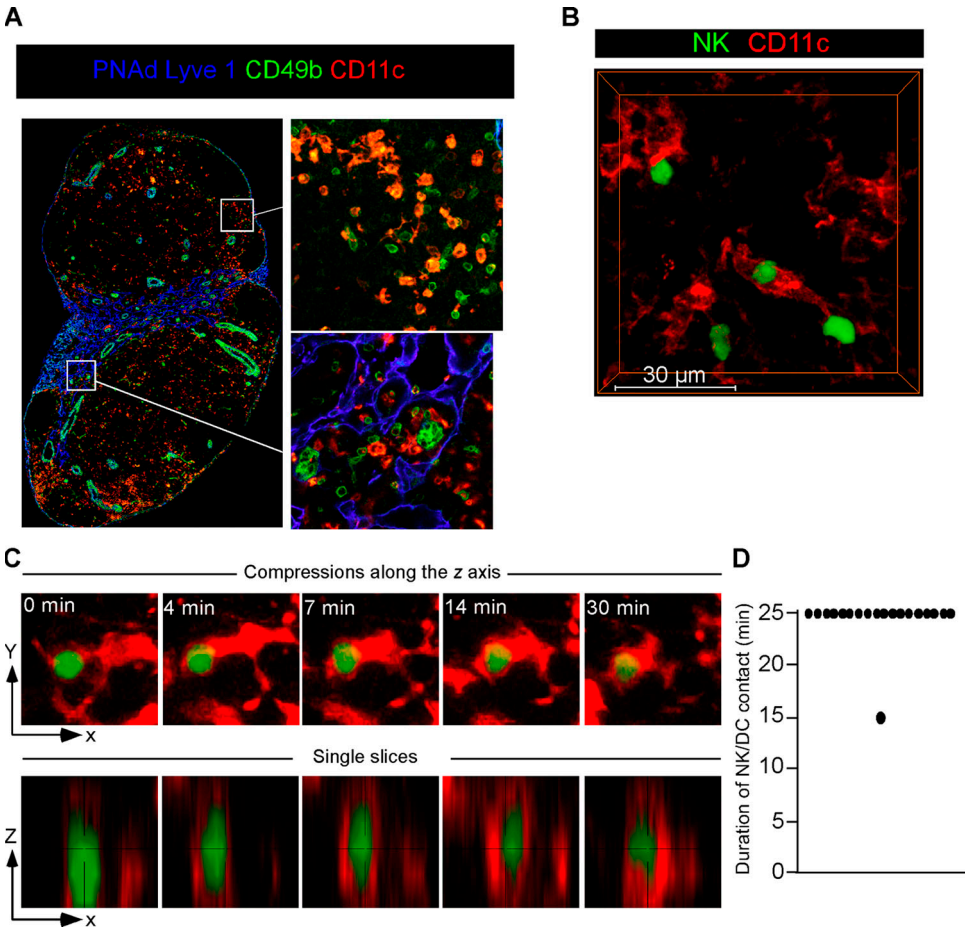

Figure 3. Colocalization and physical interaction of NK cells and DCs in LNs. (A and B) To reveal potential NK–DC interactions, LNs were collected from BALB/c mice that were either left untreated or transferred with CFSE-labeled exogenous NK cells 24 h before LN harvest. Resident DCs were visualized with CD11c staining, whereas B220 staining of B cell follicles, PNAd staining of HEVs, and Lyve-1 staining of lymphatic vessels were used to provide anatomical landmarks as in Fig. 1. Endogenous NK cells were revealed with CD49b staining (A), whereas transferred NK cells were identified by CFSE (B). (A) A section representative of 10 analyzed LNs shows colocalization of DCs and NK cells in paracortical regions below B cell follicles and in the medulla at a low magnification. The insets show enlarged images of paracortical and medullary areas where physical contacts between NK cells and DCs can be seen. (B) A three-dimensional volume representative of six examined LNs shows physical interactions between exogenously transferred NK cells and resident DCs. (C) Splenic DCs were enriched from BALB/c mice, labeled with CellTracker blue (red), and injected s.c. into recipient footpads. CFSE-labeled purified NK cells (green) were transferred i.v. into the recipients 24 h later. Mice were anesthetized 12 h later, and the popliteal LN was exposed surgically. Images were collected for 25 min in a DC-enriched area (red) where NK–DC clusters could be observed at the beginning of the imaging sessions. The rows show compression along the z axis (top) or individual slices where NK–DC contacts are unambiguous (bottom) at the indicated times within a continuous time-lapse sequence. (D) Duration of all NK–DC interactions (dots) observed.

deeper regions of the LN, where static imaging also showed these cells to be present.

Given the prolonged NK–DC interactions in the superficial LN and the fact that the resident DC network is composed of relatively immobile DCs (15), we sought to quantitatively examine the migratory behavior of NK cells. To this end, CFSE-labeled $CD3^-$ $CD49b^+$ NK cells were transferred into naive mice and analyzed using intravital imaging. CMTPX-labeled T cells were cotransferred to serve as a control, as they migrate rapidly in the LN paracortical environment (16, 17). NK cells moved slowly, exhibiting a median velocity of $v = 2.75 \pm 0.17$ μm/min while scouting relatively small areas (Fig. 4, A and B; and Video 4, available at http://www.jem.org/cgi/content/full/jem.20051474/DC1). In striking contrast, T cells displayed much higher motility with an overall median velocity of 9.6 ± 0.8 μm/min, similar to what was previously described (16, 17, 25, 26). Furthermore, although the velocity of NK cells conforms to a log normal distribution, that of T cells in the same general location is bi-log normal with two distinguishable subpopulations: 73% were highly motile ($v = 12.2 \pm 1.1$ m/min), whereas 27% exhibited a slow motility ($v = 2.75$ μm/min) comparable with that of NK cells (Fig. 4 B). Preliminary analysis indicates that the slow-moving T cell subset resides in the vicinity of the interfollicular HEV (not depicted) as suggested previously (26). Similar results were obtained when the labeling dyes for

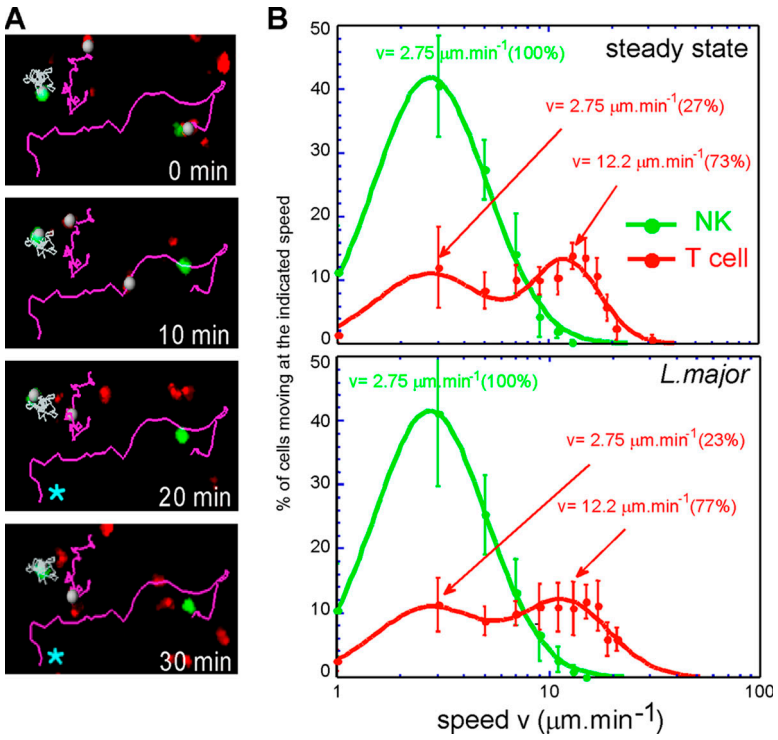

Figure 4. Intravital analysis of NK cells in LNs by 2-P microscopy. BALB/c mice were injected with CFSE-labeled NK cells (green) and CMTPX-labeled T cells (red). They were either left untreated or were infected 24 h later with *L. major* in the footpad. Animals were anesthetized 12 h later, and popliteal LNs were imaged. (A) Tracks of two T cells (purple) and one NK cell (white) during a 30-min period. These tracks are representative of each cell type. Blue stars indicate the last recorded position of the fastest T cell. (B) Velocity distribution of T cells (red line) and NK cells (green line) migrating in control LNs or LNs draining the site of *L. major* infection. Velocities were measured in three-dimensional space from point-to-point tracks at 20–30 s intervals. Four mice each were analyzed in the steady state and after infection. Error bars represent SD.

NK and T cells were reciprocally exchanged and when donor NK cells were prepared by negative selection instead of CD49b-based positive sorting (unpublished data). Therefore, the observed slow motility most likely reflects an inherent nature of NK cells, which is consistent with their prolonged physical associations with the resident DC network in the superficial LN.

NK cells are rapidly recruited from the blood to the draining LN and are induced to secrete IFN-γ upon infection with *L. major*

Close interaction between NK cells and DCs, as just described, suggests that cytokines produced by the NK cells could induce DC maturation as well as act directly on T cells colocalizing with these antigen-presenting cells. A previous study has shown that NK cells are induced to secrete IFN-γ upon infection with *L. major* (27). Therefore, we sought to visualize the NK production of IFN-γ in the draining LN of *L. major*–infected animals. Mice were injected in the ear or the hind footpad with either *L. major* or PBS, and the frequency of IFN-γ–secreting NK cells in ear-draining LNs was determined by intracellular IFN-γ staining. In infected mice, the number and frequency of $CD3^-$ $CD49b^+$ NK cells increased from 2×10^4 (0.2–0.3%) before infection to 2.5×10^5 (1.5%) 24 h after infection (Fig. 5, A and B). The frequency of IFN-γ–secreting $CD3^-$ $CD49b^+$ NK cells increased from 0.2% before infection to 20.8% at 12 h and decreased thereafter to reach 4.3% at 24 h (Fig. 5 C). Similar results were observed in the popliteal LN after injection of *L. major* into the hind footpad (not depicted). Injection of PBS into the ear did not induce an increase in the frequency of IFN-γ–secreting cells.

Two hypotheses could account for the presence of IFN-γ–secreting NK cells in the LN. First, NK cells could have been activated in the inflammatory site before their migration to the draining LN. Alternatively, their activation could have occurred in the LN. To discriminate between these two hypotheses, CFSE-labeled spleen and LN NK cells were adoptively transferred into recipient mice, which were injected with either *L. major* or PBS in each ear a day later. Mice were killed 3, 6, 9, and 12 h later, and the frequency of IFN-γ–secreting cells among $CFSE^+$ and $CFSE^-$ NK cells was measured by flow cytometry (Fig. 5 D). At each sampling time, the frequencies of IFN-γ–secreting cells among $CFSE^+$ and $CFSE^-$ $CD3^-$ $CD49b^+$ cells were comparable, suggesting that dye-labeled adoptively transferred cells behave similarly to endogenous NK cells. Furthermore, the loss of CFSE staining by NK cells was not observed up to day 3. We next investigated whether $CFSE^+$ NK cells were detected in the ears at early time points. Although $CFSE^+$ NK cells were readily found at all times in LNs and blood, they were not

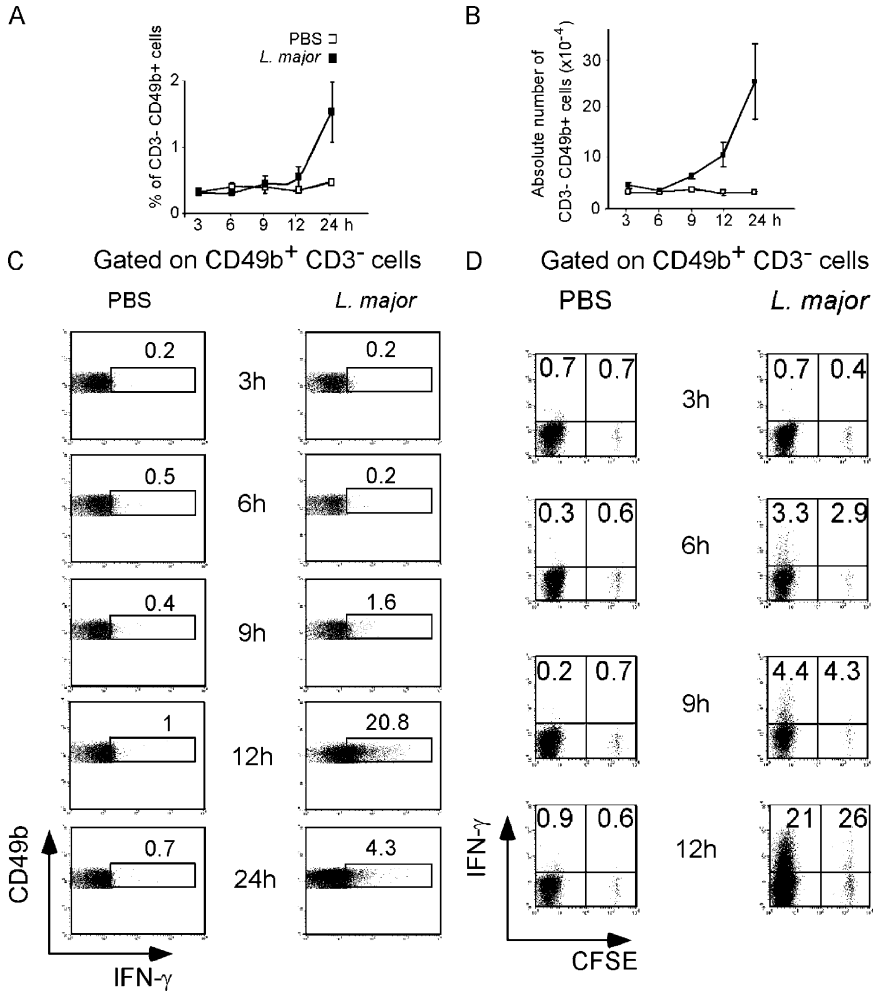

Figure 5. Rapid IFN-γ secretion by NK cells recruited from blood upon *L. major* infection. (A–C) Mice were injected with *L. major* in the left ear and PBS in the right ear, and ear-draining LNs were collected at the indicated times after infection. The frequency (A) and total number (B) of $CD3^-$ $CD49b^+$ NK cells were measured (mean ± SD [error bars]; $n = 4$). (C) The frequencies of IFN-γ producers among $CD3^-$ $CD49b^+$ NK cells were determined and are indicated in boxes for each panel. Data represent four experiments with similar results. (D) BALB/c mice were injected i.v. with CFSE-labeled NK cells followed 24 h later with *L. major* infection in the left and PBS injection in the right ear. Mice were killed at the indicated times, and LN $CD3^-$ $CD49b^+$ NK cells were analyzed by flow cytometry. Numbers in the top quadrants indicate the frequency of IFN-γ producers among endogenous $CFSE^-$ and transferred $CFSE^+$ NK cells. One of three experiments with similar results is shown.

detected in PBS-injected or in *L. major*–injected ears (Fig. S5 A, available at http://www.jem.org/cgi/content/full/jem.20051474/DC1). This latter result was confirmed by analyzing LN and ear tissue sections (not depicted). Finally, a single injection of L-selectin–blocking mAb before infection resulted in the failure of NK cells to home and accumulate in the LN in response to *L. major* (Fig. S5 B). Collectively, our data indicated that *L. major* rapidly induced both the recruitment of NK cells from the blood to the draining LN and their activation to secrete IFN-γ.

NK cells accumulate in the paracortex and rapidly secrete IFN-γ near DCs and $CD4^+$ T cells undergoing activation

We next visualized NK cells by confocal microscopy of LN sections from *L. major*–infected mice. As observed in the steady state, NK cells ($PNAd^-$ $CD49b^+$) were present in the medulla (Fig. 1 B, bottom). However, in the paracortex, NK cells accumulate under and between B cell ($B220^+$) zones (Fig. 1 A, bottom), suggesting that newly recruited NK cells accumulate in this specific region of the LN. To quantify this distribution, CFSE-labeled NK cells were injected into wild-type mice that were infected 24 h later with *L. major* in the ear. Draining LNs were harvested 12 h later, sectioned, and stained for B cell ($B220^+$) and lymphatic vessel ($Lyve\text{-}1^+$) markers (Fig. 2 a, right). Analysis of reassembled images showing an entire LN cross section indicated that in contrast to NK cells present in the LN of control mice, NK cells from infected mice tended to accumulate in the T cell area but not in the medulla. Similar numbers of NK cells were present in the medulla of control and infected mice (272 vs. 283 cells).

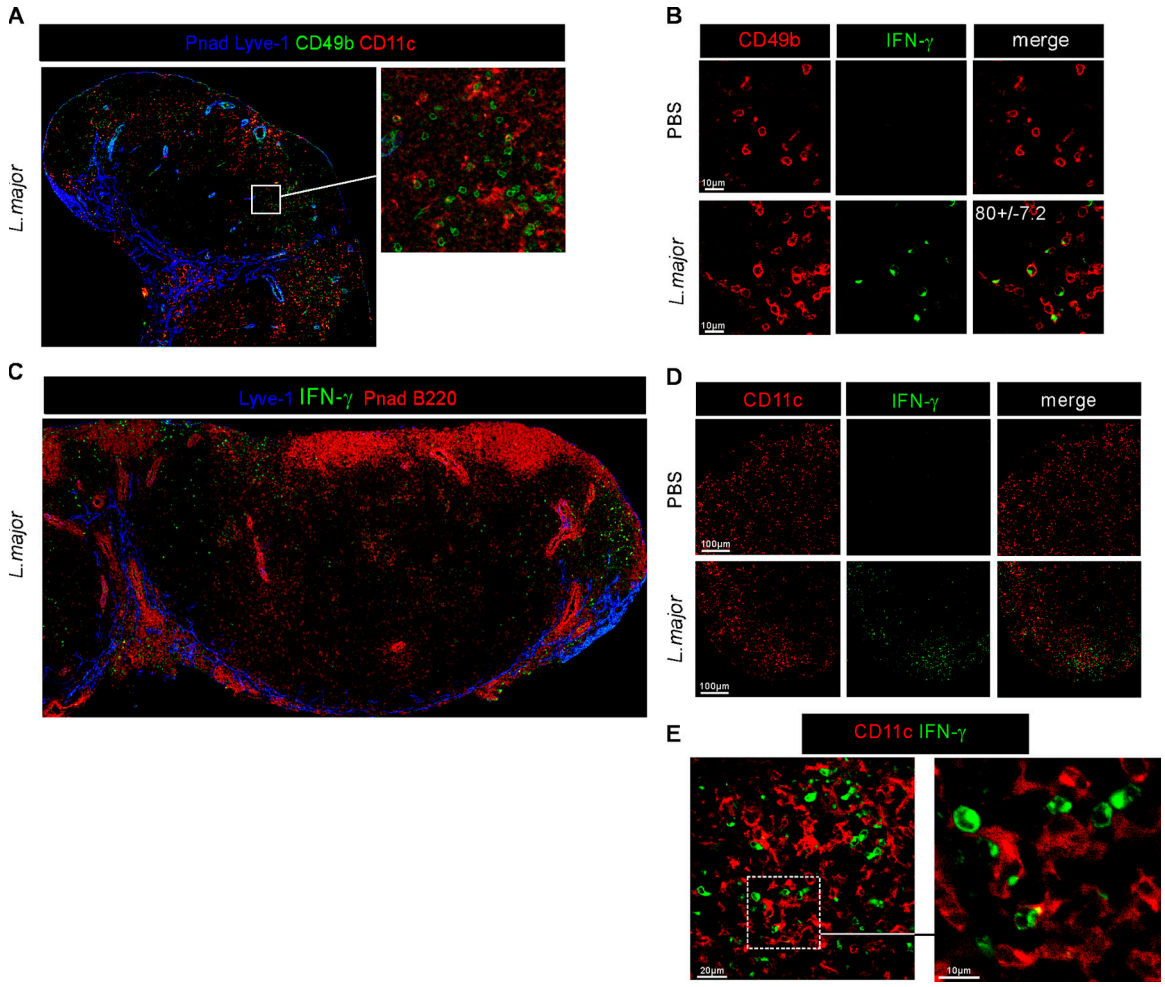

Figure 6. Specific recruitment of NK cells in the T cell zone and their associations with DCs upon *L. major* infection. BALB/c mice were injected with *L. major* in the left ear and PBS in the right ear, and tissue sections were prepared from ear-draining LNs 12 h later. (A) A representative section stained for B220, CD49b, CD11c, Lyve-1, and PNAd reveals the association of NK cells with DCs in outer paracortical areas below B cell follicles. A region where numerous NK cells and DCs were in physical contact is shown in the enlarged inset. (B) Staining for CD49b and IFN-γ demonstrates the specific induction of IFN-γ production in NK cells upon *L. major* infection. The number is the percentage of $CD49b^+$ cells among all IFN-γ producers (mean ± SD). A total of 10 LN fields were scored. (C) A representative section costained for IFN-γ, PNAd, B220, and Lyve-1 shows that IFN-γ production occurs preferentially between and under B cell follicles. (D and E) Representative sections costained for CD11c and IFN-γ show that IFN-γ producers were in close contact with DCs.

In contrast, in the T cell area, a substantial increase in NK cell number occurred in the *L. major*–infected LNs (n = 742; 72.4% of dye-labeled NK cells) compared with the control LNs (n = 211; 44% of dye-labeled NK cells). As a consequence, NK cell density in the T cell area was dramatically increased in the LN of *L. major*–infected mice (75.4 dye-labeled NK cells/mm^2) as compared with control LN (22.8 dye-labeled NK cells/mm^2).

Because NK cells colocalized with DCs in the steady state, we considered it likely that NK cells would colocalize with DCs in infected mice as well. This was indeed the case based on an analysis of LN tissue sections from infected mice after staining for CD49b, CD11c, and PNAd (Fig. 6 A). To independently confirm that NK cells interacted with DCs, CFSE-labeled NK cells were injected into naive mice. Animals were infected with *L. major*, and LNs were analyzed 12 h later by confocal microscopy after staining with anti-CD11c mAb. Out of 290 individually scored CFSE-labeled NK cells, 158 (55%) were in contact with large $CD11c^+$ cells.

L. major induced the activation of NK cells and their specific recruitment under the B cell follicles of the T cell zone, the so-called cortical ridge where T cell activation occurs (28). *L. major* also induced IFN-γ secretion by NK cells, a process that was recently shown to play a role in the differentiation of naive $CD4^+$ T cells into Th1 effector cells. As a first step to investigate whether IFN-γ secretion by NK cells could play a role in the differentiation of parasite-specific $CD4^+$ T cells, we examined the distribution of IFN-γ–secreting NK cells in the LNs of infected mice. Mice were injected with either *L. major* or PBS, and LN sections were analyzed 12 h later

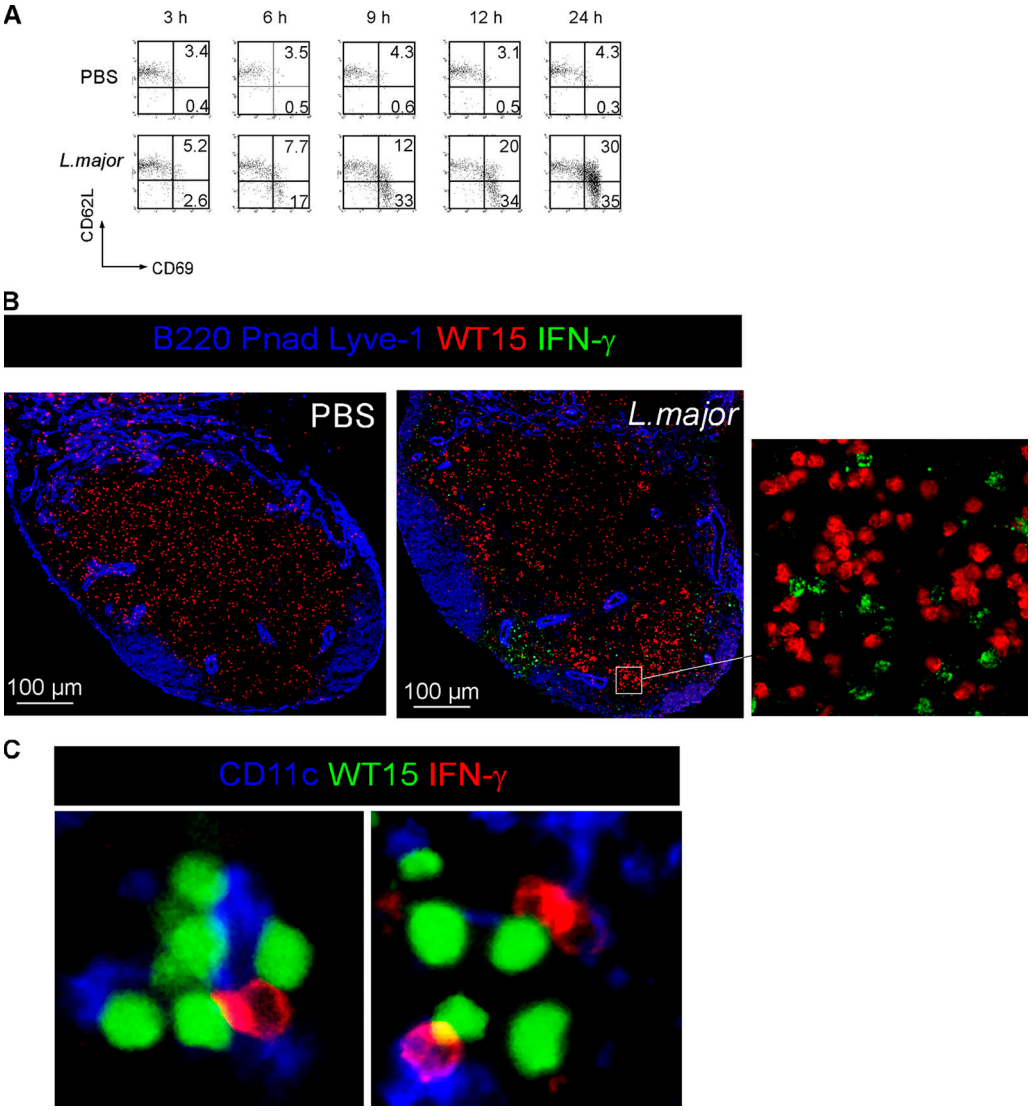

Figure 7. Distribution of NK cells, IFN-γ–secreting cells, and parasite-specific CD4$^+$ T cells in LNs. CD90.1$^+$ CD4$^+$ cells from WT15 TCR transgenic mice were labeled with CFSE and injected into CD90.1$^-$ BALB/c mice. Recipient mice were injected 24 h later with *L. major* in the right ear and PBS in the left ear. (A) The activation status of WT15 cells was examined by flow cytometry at the indicated times upon staining with anti-CD62L and anti-CD69 mAb. Data show dot plots after gating on CD90.1$^+$ cells and are representative of three experiments. Numbers indicate the percentage of cells in each quadrant. (B and C) Mice were killed 12 h after injection, and the distribution of WT15 cells and IFN-γ–secreting NK cells was analyzed on LN sections after staining for B220, PNAd, Lyve-1, and IFN-γ. (B) Representative sections are shown, and the inset shows the colocalization of CD4 T cells undergoing activation and IFN-γ–secreting cells. (C) Pictures show clusters of CD11c$^+$ DCs, WT15 cells, and IFN-γ–secreting cells. (A–C) A total of 10 LNs were examined for each infection and control condition.

by confocal microscopy after staining with anti–IFN-γ, anti-CD49b, and anti-CD11c mAb. Staining with anti–IFN-γ mAb was observed on LN tissue sections from *L. major*–infected but not from PBS-injected animals. The majority (80 ± 7.2%) of IFN-γ–secreting cells were CD49b$^+$, and these cells exhibited intracellular IFN-γ staining (Fig. 6 B). IFN-γ–secreting cells were localized in the paracortex but rarely in the medulla, indicating that their activation mainly took place in the paracortex, where they were recruited (Fig. 6 C). IFN-γ–secreting cells were also present in DC-rich areas (Fig. 6 D) and were in contact with DCs (Fig. 6 E).

Interfollicular as well as deeper paracortex regions are rich in HEVs. Antigen-loaded DCs settle next to HEVs, allowing them to trap antigen-specific CD4$^+$ T cells entering LNs through these sites (28, 29). To visualize IFN-γ–secreting NK cells and CD4$^+$ T cell activation in vivo, CD90.1$^+$ WT15 TCR transgenic T cells were labeled with CFSE and injected into CD90.1$^-$ BALB/c mice. Mice were infected with *L. major*, and CD90.1$^+$ LN cells were analyzed by flow cytometry after staining with anti-CD69 and anti-CD62L mAb. CD69$^+$ and/or CD62L^{low} TCR transgenic T cells were first detected in ear-draining LNs 6 h

after infection and did not divide until at least 24 h (Fig. 7 A and not depicted). Therefore, IFN-γ secretion by NK cells and parasite-induced T cell activation occurred at the same time in draining LNs. Analysis of LN tissue sections after staining with anti-PNAd and anti-B220 mAb revealed that the activation of TCR transgenic T cells mainly occurred beneath B cell follicles in infected animals (Fig. 7 B). Staining with anti–IFN-γ mAb further showed that TCR transgenic T cells and IFN-γ–secreting cells were found in the same area and contacted the same DC in *L. major*–infected mice (Fig. 7 C). Collectively, these results showed that IFN-γ–secreting NK cells, DCs, and $CD4^+$ T cells undergoing activation were localized to and able to interact in the same region of the LN. This location could allow NK cells to provide an early source of IFN-γ and influence differentiation of the activated T cells, as recently suggested in another experimental model (10).

Static imaging revealed changes in the global distribution of activated NK cells in the LNs of *L. major*–infected mice, so these activated cells might show dynamic behavior that would differ from the slow localized motility of resting NK cells in naive animals. Intravital imaging of LNs in infected mice, however, revealed that *L. major* infection did not have a detectable effect on NK cell and T cell motility (Fig. 4 B and Video 5, available at http://www.jem.org/cgi/content/full/jem.20051474/DC1). As in naive animals, physical contacts between NK cells and MHC class II–positive cells were prolonged in LNs of infected mice, with 96% of NK cells remaining in contact with those cells for >20 min (Video 6 and not depicted). Finally, at later time points, NK cells remained localized in the paracortex and medulla (Fig. S6).

DISCUSSION

We have used immunostaining in tissue sections and intravital 2-P microscopy to monitor the localization and dynamic behavior of NK cells in LNs in the steady state and upon infection with *L. major*. In the steady state, NK cells distributed in nearly equal numbers to both the paracortex and medulla. Upon infection with *L. major*, NK cells were rapidly recruited from the blood via the HEV and accumulated under the B cell follicles, where they produced IFN-γ. This region of the paracortex is the area where primary afferent lymphatics and the conduit system that drains lymph are dense (28). NK cells can be activated by cellular contacts (4, 30, 31) and soluble signals such as type I IFN, IL-12, IL-18, or IL-2 (9, 32). Therefore, the strategic location and recruitment of NK cells to the paracortex could allow these cells to rapidly interact with and eventually be activated by lymph- and blood-borne cells and soluble molecules entering the LN parenchyma in this zone and activating resident DCs. The medulla is the region of the LN where lymphatics anastomose before lymph exits the LN. The location of NK cells in this region does not have an obvious relationship to function during infection. Although our data indicate that NK cells show little motility under steady-state conditions, it is possible that there is a slow rate of entry and exit from the LN and that the NK cells in the medulla represent an accumulation of cells exiting the LN.

Using in vivo 2-P microscopy, we have found that like DCs, NK cells were relatively immotile in the superficial LN paracortex. This is in striking contrast to other lymphoid cells in this tissue, especially naive T cells. The paracortex exhibits a complex architecture with fibroblastic reticular cell–delineated corridors (12, 28). The location of NK cells in this highly structured region could, therefore, contribute to the restricted motility of NK cells, although this is unlikely to be the only explanation given that many T cells in the same area show much higher velocities (Video 7, available at http://www.jem.org/cgi/content/full/jem.20051474/DC1). So why do NK cells in this region move slowly? This behavior could be an intrinsic feature of this cell type and/or be imposed by their microenvironment. Previous studies have shown that NK cells proliferated when injected into NK cell–deficient but not T cell–deficient recipients, suggesting that NK cells occupy specific niches within the lymphoid organs (33, 34). Interestingly, IL-15, the main NK survival signal molecule, is expressed by mature DCs (9). Therefore, the fact that NK cells exhibit long-lasting contacts with DCs raises the possibility that this interaction both promotes NK cell survival and also signals for the cessation of NK cell migration, resulting in the accumulation of these cells in a critical region of the LN.

Why should T cells and NK cells exhibit such different migratory dynamics? In contrast to NK cells, T cells express unique antigen-specific TCRs. Therefore, it makes sense for T cells to continuously sample different antigen-presenting cells to increase the probability that they will encounter their cognate ligand. In contrast to T cells, NK cells express multiple overlapping receptors and exhibit a constitutively demethylated IFN-γ locus (35, 36). One main function of NK cells in LNs could be to secrete IFN-γ in direct or indirect response to inflammatory stimuli draining to the LN from a peripheral site of infection. This is in accord with the finding that only human $CD56^{bright}$ NK cells, which are specialized in the production of cytokines, localize in LNs (8). The ability to rapidly produce cytokines in a nonclonal manner would allow a prepositioned and a newly recruited NK cell network to respond to lymph-borne signals without the need to be motile as part of a search strategy for detection of rare, specific ligands.

Studies have shown that DCs activate NK cells and that NK cells can influence DC maturation in vitro (5, 32, 37). However, direct evidence showing that NK cells and DCs interact in vivo has been lacking. In this study, we have shown that NK cells make long and stable contacts with DCs in the LN paracortex both in the steady state and upon *L. major* infection. Interestingly, resident DCs form a rather sessile network that enmeshes DCs arriving in the LN from peripheral tissue (15). Because NK cell and DC networks are tightly interconnected, this provides an opportunity for incoming DCs to activate resident NK cells. Finally, NK cell–derived IFN-γ is important for $CD4^+$ T cell Th1

differentiation (10, 27, 38). In *L. major*–infected mice, we have shown that both parasite-specific $CD4^+$ T cells and NK cells accumulated in the outer paracortex beneath B cell follicles at a time when NK cells secreted high amounts of IFN-γ. Activated DCs that home to LNs can activate T cells and have been shown to promote NK cell recruitment in the same LN. Therefore, DC recruitment to the draining LN after *L. major* infection could induce NK recruitment at a time when and in a location where T cell activation is occurring, thus orchestrating the encounter of T and NK cells during their activation. Colocalization of both cell types during initiation of the immune response could allow IFN-γ derived from NK cells to influence $CD4^+$ T cell differentiation as previously reported (10). Thus, together with published data (2, 5, 9, 10, 38), the new results reported here provide a framework for understanding the role of NK cells in the early development of adaptive immune responses within secondary lymphoid tissues.

MATERIALS AND METHODS

Mice and parasites. BALB/c mice were purchased from Charles River Laboratories. I-Aβ-EGFP transgenic mice (24) were obtained from the National Institute of Allergy and Infectious Diseases (NIAID) contract facility at Taconic. WT15 TCR transgenic mice have been previously described (39). Animals were housed under specific pathogen-free conditions and used between 7 and 10 wk of age. *L. major* promastigotes (World Health Organization strain WHOM/IR/-/173) were grown in M199 medium containing 20% FCS. Mice were infected with 2×10^6 stationary phase promastigotes in the ears of anesthetized mice. All experiments were performed in compliance with institutional guidelines and have been approved by the local committee for animal experimentation.

Reagents and antibodies. Rabbit anti–mouse/rat asialo GM1 polyclonal antibody was purchased from Cedarlane. Whole Rat IgG was purchased from Pierce Chemical Co. The following mAbs were purchased from Becton Dickinson: RM4-5, anti-CD4, RA3-6B2, anti-B220, HL3, anti-CD11c, MECA-79, anti-PNAd, XMG1.2, anti–IFN-γ, M1.70, anti-CD11b, DX5, HMα2, anti-CD49b, 145 2C11, anti-CD3, MEL-14, and anti-CD62L. Anti–Lyve-1 polyclonal antibody was purchased from Acris Antibodies. These mAbs were used either uncoupled or conjugated with allophycocyanin, PE, FITC, and AlexaFluor488 or 647. Purified mAbs were revealed using the appropriate AlexaFluor488-, 568-, or 647-conjugated anti-Ig antibodies (Invitrogen).

Intracellular IFN-γ staining of NK cells. Cells were stained with anti-CD3 and anti-CD49b mAb, fixed with Cytofix buffer (Becton Dickinson), and incubated with Cytoperm permeabilization buffer (Becton Dickinson) containing anti–IFN-γ mAb.

Adoptive transfer. For polyclonal T cells, LN cells were negatively isolated using a pan T cell isolation kit (Miltenyi Biotec) labeled with 5 μM of either CMTPX, CFSE, CMTMR, or SNARF-1 (Invitrogen). They were then washed and injected i.v. into recipient mice (3×10^6 cells/mouse). $CD3^+$ T cells were >99% pure. For WT15 TCR transgenic $CD4^+$ T cells, LN cells were negatively isolated using anti–class II, anti-CD8α, anti-B220, and anti-CD11b mAb followed by sheep anti–rat magnetic beads (Dynal). $CD4^+$ T cells were 96–98% pure. T cells were labeled with 5 μM of either orange fluorescent tetramethyrhodamine (CMTMR) or CFSE, washed, and injected i.v. into recipient mice (3×10^6 cells/mouse). For NK cells, spleen and LN cells were enriched for $CD49b^+$ cells using DX5-coated magnetic beads (Miltenyi Biotec). Cells were stained with anti-CD3 and anti-CD49b mAb, and $CD3^-$ $CD49b^+$ cells were sorted by flow cytometry. Cells were labeled with 5 μM of either CMPTX or CFSE, washed, and injected i.v. into recipient mice ($2.5–5 \times 10^6$ cells/mouse). For DC visualization experiments, splenic cells were enriched for $CD11c^+$ cells using CD11c-coated magnetic beads (Miltenyi Biotec). DC purity was routinely >95%. Cells were labeled with 75 μM of CellTracker blue (Invitrogen), washed, and injected s.c. into recipient mice hind footpads (10^6 cells/footpad).

Immunofluorescence. LNs were fixed overnight in medium containing 0.05 M phosphate buffer, 0.1 M L-lysine, pH 7.4, 2 mg/ml $NaIO_4$, and 10 mg/ml paraformaldehyde and were dehydrated in consecutive sucrose gradients (10, 20, and 30% in phosphate buffer). Tissues were snap frozen in Tissue-Tek (Sakura Finetek). 8-μm frozen sections were stained with either FITC or allophycocyanin anti-B220 antibody (RA36B2), AlexaFluor488, 568, or 647 phalloidin (Invitrogen), unconjugated anti-PNAd antibody (MECA-79), allophycocyanin anti-CD11c antibody (HL3), AlexaFluor647 anti-CD49b (HMα2), and unconjugated or AlexaFluor647 anti–IFN-γ (XMG1.2) as previously described (40). PNAd and IFN-γ staining was revealed with an AlexaFluor647 goat anti–rat IgG (Invitrogen). Immunofluorescence confocal microscopy was performed with a confocal microscope (model TCS P; Leica). Separate images were collected for each fluorochrome and overlaid to obtain a multicolor image. Individual fields of an LN section were scanned, and the different images were juxtaposed to reconstitute the image of a whole LN cross section. Final image processing was performed using Adobe Photoshop. Quantitative analysis of NK cell density in the T cell area and the medulla in LN sections was performed using ImageJ software (National Institutes of Health).

2-P microscopy. Freshly isolated fluorescent dye-labeled NK cells (5 μM CFSE) and polyclonal T cells (5 μM CMTPX) were injected i.v. into BALB/c recipient mice. Animals were infected or uninfected with *L. major* as indicated. After anesthetization, the right popliteal LN was surgically exposed and imaged with a multiphoton system (Radiance 2100; Bio-Rad Laboratories) equipped with an upright microscope (model 600 FN; Nikon) fitted with a 20× water immersion lens (NA 0.95; Olympus). The 2-P laser was either an Sa-Ti femtosecond pulsed laser (Mira900; Coherent) tuned to 800 nM that was driven by a 10-W pump laser (Verdi; Coherent) or a femtosecond pulsed laser (Chameleon-XR; Coherent) tuned to 880 nm. Images in videos were collected with a typical voxel size of $0.91 \times 0.91 \times 5$ μm and a volume dimension of $466 \times 466 \times 50–100$ μm unless indicated otherwise. Images were typically collected between 50–140 μM below the capsule as indicated for each video. This volume collection was repeated every 20–30 s to create four-dimensional datasets that were then processed with Imaris software (Bitplane) and AfterEffect (Adobe). All supplemental videos play back at 300× real time. Data were analyzed and fitted with a bi-log normal distribution yielding the weight $\alpha_\iota/(\alpha_1 + \alpha_2)$ and the mode ν of each distribution.

Online supplemental material. Fig. S1 shows NK cell labeling in tissue sections. Fig. S2 shows that splenic and LN NK cells home to LNs upon adoptive transfer, and Fig. S3 shows that NK cells home to LNs via HEVs. Fig. S4 shows NK cell behavior in class II GFP^+ mice. Fig. S5 shows that NK cells do not home to infected tissue before their activation within LNs. Fig. S6 is a picture of a representative dLN harvested 6 d after *L. major* injection and stained for Lyve-1, PNAd, B220, and CD49b. Video 1 is an animation of the three-dimensional volume shown in Fig. 3 B that displays in more detail the interactions between the CFSE-labeled NK cells and the endogenous DCs. Video 2 shows NK cells that were purified from C57Bl/6 mice, stained with SNARF-1, and injected i.v. into I-Aβ-EGFP transgenic mice. Video 3 shows splenic DCs that were enriched from BALB/c mice, labeled with CellTracker blue, and injected s.c. into recipient footpads. Video 4 shows CFSE-labeled NK cells and CMTPX-labeled T cells that were injected i.v. into recipient BALB/c mice, whereas Video 5 shows these mice injected 24 h later with *L. major* in the footpad. Video 6 shows NK cells that were purified from C57Bl/6 mice, stained with SNARF-1, and injected i.v. into I-Aβ-EGFP transgenic mice that were injected 24 h later in the

footpad with *L. major*. Video 7 was obtained by processing the same raw data as for Video 4. Online supplemental material is available at http://www.jem.org/cgi/content/full/jem.20051474/DC1.

We thank Corinne Schricke for skilled technical help, Nathan Peters and David Sacks (NIAID, Bethesda, MD) for providing us with cultures of *L. major*, and Jackson Egen, Grégoire Altan-Bonnet, and Frédéric Brau for advice and help.

This work was supported by grants from the Ministère de l'Education Nationale, de la Recherche et de l'Enseignement Supérieur, the Fondation pour la Recherche Médicale, the Association pour la Recherche contre le Cancer, and funds from the Intramural Research Program of the National Institutes of Health NIAID. A.Y.C. Huang and H. Qi were supported by postdoctoral fellowship grants from the Cancer Research Institute.

The authors have no conflicting financial interests.

Submitted: 23 July 2005
Accepted: 1 February 2006

REFERENCES

1. French, A.R., and W.M. Yokoyama. 2003. Natural killer cells and viral infections. *Curr. Opin. Immunol.* 15:45–51.
2. Yokoyama, W.M., S. Kim, and A.R. French. 2004. The dynamic life of natural killer cells. *Annu. Rev. Immunol.* 22:405–429.
3. Fernandez, N.C., A. Lozier, C. Flament, P. Ricciardi-Castagnoli, D. Bellet, M. Suter, M. Perricaudet, T. Tursz, E. Maraskovsky, and L. Zitvogel. 1999. Dendritic cells directly trigger NK cell functions: cross-talk relevant in innate anti-tumor immune responses in vivo. *Nat. Med.* 5:405–411.
4. Piccioli, D., S. Sbrana, E. Melandri, and N.M. Valiante. 2002. Contact-dependent stimulation and inhibition of dendritic cells by natural killer cells. *J. Exp. Med.* 195:335–341.
5. Gerosa, F., B. Baldani-Guerra, C. Nisii, V. Marchesini, G. Carra, and G. Trinchieri. 2002. Reciprocal activating interaction between natural killer cells and dendritic cells. *J. Exp. Med.* 195:327–333.
6. Ferlazzo, G., M.L. Tsang, L. Moretta, G. Melioli, R.M. Steinman, and C. Munz. 2002. Human dendritic cells activate resting natural killer (NK) cells and are recognized via the NKp30 receptor by activated NK cells. *J. Exp. Med.* 195:343–351.
7. Andrews, D.M., A.A. Scalzo, W.M. Yokoyama, M.J. Smyth, and M.A. Degli-Esposti. 2003. Functional interactions between dendritic cells and NK cells during viral infection. *Nat. Immunol.* 4:175–181.
8. Fehniger, T.A., M.A. Cooper, G.J. Nuovo, M. Cella, F. Facchetti, M. Colonna, and M.A. Caligiuri. 2003. CD56bright natural killer cells are present in human lymph nodes and are activated by T cell-derived IL-2: a potential new link between adaptive and innate immunity. *Blood.* 101:3052–3057.
9. Ferlazzo, G., M. Pack, D. Thomas, C. Paludan, D. Schmid, T. Strowig, G. Bougras, W.A. Muller, L. Moretta, and C. Munz. 2004. Distinct roles of IL-12 and IL-15 in human natural killer cell activation by dendritic cells from secondary lymphoid organs. *Proc. Natl. Acad. Sci. USA.* 101:16606–16611.
10. Martin-Fontecha, A., L.L. Thomsen, S. Brett, C. Gerard, M. Lipp, A. Lanzavecchia, and F. Sallusto. 2004. Induced recruitment of NK cells to lymph nodes provides IFN-gamma for T(H)1 priming. *Nat. Immunol.* 5:1260–1265.
11. Blaschke, V., B. Micheel, R. Pabst, and J. Westermann. 1995. Lymphocyte traffic through lymph nodes and Peyer's patches of the rat: B- and T-cell-specific migration patterns within the tissue, and their dependence on splenic tissue. *Cell Tissue Res.* 282:377–386.
12. Gretz, J.E., A.O. Anderson, and S. Shaw. 1997. Cords, channels, corridors and conduits: critical architectural elements facilitating cell interactions in the lymph node cortex. *Immunol. Rev.* 156:11–24.
13. Gretz, J.E., C.C. Norbury, A.O. Anderson, A.E. Proudfoot, and S. Shaw. 2000. Lymph-borne chemokines and other low molecular weight molecules reach high endothelial venules via specialized conduits while a functional barrier limits access to the lymphocyte microenvironments in lymph node cortex. *J. Exp. Med.* 192:1425–1440.
14. Baekkevold, E.S., T. Yamanaka, R.T. Palframan, H.S. Carlsen, F.P. Reinholt, U.H. von Andrian, P. Brandtzaeg, and G. Haraldsen. 2001. The CCR7 ligand elc (CCL19) is transcytosed in high endothelial venules and mediates T cell recruitment. *J. Exp. Med.* 193:1105–1112.
15. Lindquist, R.L., G. Shakhar, D. Dudziak, H. Wardemann, T. Eisenreich, M.L. Dustin, and M.C. Nussenzweig. 2004. Visualizing dendritic cell networks in vivo. *Nat. Immunol.* 5:1243–1250.
16. Miller, M.J., S.H. Wei, I. Parker, and M.D. Cahalan. 2002. Two-photon imaging of lymphocyte motility and antigen response in intact lymph node. *Science.* 296:1869–1873.
17. Miller, M.J., S.H. Wei, M.D. Cahalan, and I. Parker. 2003. Autonomous T cell trafficking examined in vivo with intravital two-photon microscopy. *Proc. Natl. Acad. Sci. USA.* 100:2604–2609.
18. Sacks, D., and N. Noben-Trauth. 2002. The immunology of susceptibility and resistance to *Leishmania major* in mice. *Nat. Rev. Immunol.* 2:845–858.
19. Dokun, A.O., D.T. Chu, L. Yang, A.S. Bendelac, and W.M. Yokoyama. 2001. Analysis of in situ NK cell responses during viral infection. *J. Immunol.* 167:5286–5293.
20. Andrews, D.M., H.E. Farrell, E.H. Densley, A.A. Scalzo, G.R. Shellam, and M.A. Degli-Esposti. 2001. NK 1.1+ cells and murine cytomegalovirus infection: what happens in situ? *J. Immunol.* 166:1796–1802.
21. Arase, H., T. Saito, J.H. Phillips, and L.L. Lanier. 2001. Cutting edge: the mouse NK cell-associated antigen recognized by DX5 monoclonal antibody is CD49b (alpha 2 integrin, very late antigen-2). *J. Immunol.* 167:1141–1144.
22. Hemmerich, S., E.C. Butcher, and S.D. Rosen. 1994. Sulfation-dependent recognition of high endothelial venules (HEV)-ligands by L-selectin and MECA 79, and adhesion-blocking monoclonal antibody. *J. Exp. Med.* 180:2219–2226.
23. Gallatin, W.M., I.L. Weissman, and E.C. Butcher. 1983. A cell-surface molecule involved in organ-specific homing of lymphocytes. *Nature.* 304: 30–34.
24. Boes, M., J. Cerny, R. Massol, M. Op den Brouw, T. Kirchhausen, J. Chen, and H.L. Ploegh. 2002. T-cell engagement of dendritic cells rapidly rearranges MHC class II transport. *Nature.* 418:983–988.
25. Mempel, T.R., S.E. Henrickson, and U.H. Von Andrian. 2004. T-cell priming by dendritic cells in lymph nodes occurs in three distinct phases. *Nature.* 427:154–159.
26. Huang, A.Y., H. Qi, and R.N. Germain. 2004. Illuminating the landscape of in vivo immunity: insights from dynamic in situ imaging of secondary lymphoid tissues. *Immunity.* 21:331–339.
27. Scharton-Kersten, T., and P. Scott. 1995. The role of the innate immune response in Th1 cell development following *Leishmania major* infection. *J. Leukoc. Biol.* 57:515–522.
28. Katakai, T., T. Hara, J.H. Lee, H. Gonda, M. Sugai, and A. Shimizu. 2004. A novel reticular stromal structure in lymph node cortex: an immuno-platform for interactions among dendritic cells, T cells and B cells. *Int. Immunol.* 16:1133–1142.
29. Bajenoff, M., S. Granjeaud, and S. Guerder. 2003. The strategy of T cell antigen-presenting cell encounter in antigen-draining lymph nodes revealed by imaging of initial T cell activation. *J. Exp. Med.* 198: 715–724.
30. Ferlazzo, G., C. Semino, M. Meta, F. Procopio, B. Morandi, and G. Melioli. 2002. T lymphocytes express B7 family molecules following interaction with dendritic cells and acquire bystander costimulatory properties. *Eur. J. Immunol.* 32:3092–3101.
31. Moretta, L., R. Biassoni, C. Bottino, M.C. Mingari, and A. Moretta. 2002. Surface receptors that regulate the NK cell function: beyond the NK cell scope. *Curr. Top. Microbiol. Immunol.* 266:11–22.
32. Granucci, F., I. Zanoni, N. Pavelka, S.L. Van Dommelen, C.E. Andoniou, F. Belardelli, M.A. Degli Esposti, and P. Ricciardi-Castagnoli. 2004. A contribution of mouse dendritic cell-derived IL-2 for NK cell activation. *J. Exp. Med.* 200:287–295.
33. Ranson, T., C.A. Vosshenrich, E. Corcuff, O. Richard, W. Muller, and J.P. Di Santo. 2003. IL-15 is an essential mediator of peripheral NK-cell homeostasis. *Blood.* 101:4887–4893.
34. Cooper, M.A., J.E. Bush, T.A. Fehniger, J.B. VanDeusen, R.E. Waite, Y. Liu, H.L. Aguila, and M.A. Caligiuri. 2002. In vivo evidence for a dependence on interleukin 15 for survival of natural killer cells. *Blood.* 100:3633–3638.

35. Stetson, D.B., M. Mohrs, R.L. Reinhardt, J.L. Baron, Z.E. Wang, L. Gapin, M. Kronenberg, and R.M. Locksley. 2003. Constitutive cytokine mRNAs mark natural killer (NK) and NK T cells poised for rapid effector function. *J. Exp. Med.* 198:1069–1076.
36. Tato, C.M., G.A. Martins, F.A. High, C.B. DiCioccio, S.L. Reiner, and C.A. Hunter. 2004. Cutting edge: innate production of IFN-gamma by NK cells is independent of epigenetic modification of the IFN-gamma promoter. *J. Immunol.* 173:1514–1517.
37. Moretta, A. 2002. Natural killer cells and dendritic cells: rendezvous in abused tissues. *Nat. Rev. Immunol.* 2:957–964.
38. Scharton, T.M., and P. Scott. 1993. Natural killer cells are a source of interferon γ that drives differentiation of CD4+ T cell subsets and induces early resistance to *Leishmania major* in mice. *J. Exp. Med.* 178:567–577.
39. Wang, Q., L. Malherbe, D. Zhang, K. Zingler, N. Glaichenhaus, and N. Killeen. 2001. CD4 promotes breadth in the TCR repertoire. *J. Immunol.* 167:4311–4320.
40. Bajenoff, M., and S. Guerder. 2003. Homing to nonlymphoid tissues is not necessary for effector Th1 cell differentiation. *J. Immunol.* 171:6355–6362.